UNIVERSITEIT
AMSTERDAM

VU Research Portal

Combustion synthesis of metal carbides: Part I. Model development

Locci, A.M.; Cincotti, A.; Delogu, F.; Orru, R.V.A.; Cao, G.

Link to publication in VU Research Portal

Combustion synthesis of metal carbides: Part I. Model development

A.M. Locci, A. Cincotti[a)], F. Delogu, and R. Orrù
Dipartimento di Ingegneria Chimica e Materiali, Centro Studi sulle Reazioni Autopropaganti (CESRA), Unità di Ricerca del Consorzio Interuniversitario Nazionale di Scienza e Tecnologia dei Materiali (INSTM), Università degli Studi di Cagliari, 09123 Cagliari, Italy

G. Cao[b)]
Dipartimento di Ingegneria Chimica e Materiali, Centro Studi sulle Reazioni Autopropaganti (CESRA), Unità di Ricerca del Consorzio Interuniversitario Nazionale di Scienza e Tecnologia dei Materiali (INSTM), Università degli Studi di Cagliari, 09123 Cagliari, Italy; and CRS4, Parco Scientifico e Tecnologico, POLARIS, 09010 Pula (CA), Italy

The definition of a rigorous theoretical framework for the appropriate physico-chemical description of self-propagating high-temperature synthesis (SHS) processes represents the main goal of this work which is presented in two sequential articles. In this article, a novel mathematical model to simulate SHS processes is proposed. By adopting a heterogeneous approach for the description of mass transfer phenomena, the model is based on appropriate mass and energy conservation equations for each phase present during the system evolution. In particular, it takes microstructural evolution into account using suitable population balances and properly evaluating the different driving forces from the relevant phase diagram. The occurrence of phase transitions is treated on the basis of the so-called enthalpy approach, while a conventional nucleation-and-growth mechanistic scenario is adopted to describe quantitatively the formation of reaction products. The proposed mathematical model may be applied to the case of combustion synthesis processes involving a low melting point reactant and a refractory one, as for the synthesis of transition metal carbides from pure metal and graphite. Thus, the model can be profitably used to gain a deeper insight into the microscopic elementary phenomena involved in combustion synthesis processes through a suitable combination of experimental and modeling investigations, as it may be seen in Part II of this work [J. Mater. Res. **20,** 1269 (2005)].

I. INTRODUCTION

It is well known that the large heat release associated with the chemical conversion of reactants in products in highly exothermic systems can give rise to self-sustaining reactions.[1] Irrespective of the gaseous, liquid, or solid nature of reactant species, the experimental setup can be suitably arranged to allow the generation of high-temperature combustion waves. Due to system exothermicity and consequent self-sustaining characteristics of the process, combustion waves are able to self-propagate along directions which depend upon experimental conditions.[2] The combustion process involving solid phase reactants and products is generally referred to as self-propagating high-temperature synthesis (SHS). Since the early 1970s, it has been used for the preparation of advanced materials, such as intermetallics, ceramics, and composites.[3]

According to the picture emerging from about three decades of intense research and studies, SHS is a complex process involving a considerable number of interrelated phenomena, including the formation of molten phases as well as of final solid products and their subsequent microstructural evolution.[4] It is therefore not surprising that the mathematical description of self-propagating combustion processes requires a considerable degree of sophistication.[5,6]

At the beginning of the 1960s, the self-sustaining exothermic processes in condensed phases were phenomenologically treated in the framework of the classical combustion theory.[7] Taking advantage of both the so-called thin-reaction-zone hypothesis and the Frank–Kamenetskii approximation, several homogeneous mod-

---

Address all correspondence to these authors.
[a)]e-mail: cincotti@visnu.dicm.unica.it
[b)]e-mail: cao@visnu.dicm.unica.it

els have been developed, yielding analytical expressions for the front velocity as a function of an effective activation energy of the combustion reaction.[8–10] The dependence of the combustion wave velocity on factors as diverse as the reactant particle size, the mixture stoichiometry, and the initial temperature was analytically worked out under various approximations and assumptions[11] while a suitable numerical integration provided the spatial-temporal profiles of both temperature and conversion degrees. Furthermore, homogeneous models have been extensively adopted to investigate the stability of combustion wave propagation.[12–16]

The limitations connected with the use of homogeneous models were easily recognized and inspired subsequent research works. Heterogeneous models were soon developed to account for interphase material transport[17] and melting phenomena,[18] which have a strong influence on the combustion rate as a consequence of the increased contact area among reactants. Following a different approach, so-called cellular models were also developed.[19] Based on the tessellation of the reaction medium with elementary cells interacting through given sets of rules, such models evidenced the dependence of the shape and the propagation rate of the combustion wave on the micro-heterogeneity of the reacting mixture.[20]

In particular, various heterogeneous approaches for modeling important features such as the use of phase diagrams for driving forces evaluation,[21] the incorporation of dissolution and precipitation kinetics in reaction mechanism,[22] the quantitative description of microstructure evolution,[23] etc., have been adopted. However, a thorough model that properly treats in a comprehensive manner the mathematical description of all these phenomena was still missing.

The only attempt to deal with a complete description of system thermodynamics and kinetics was worked out by Stangle and co-workers in the early 1990s.[24] The mathematical model was applied to the case of SHS processes involving a low melting point reactant and a refractory one, as in the synthesis of transition metal carbides from pure metal and graphite.[25] The possible occurrence of phase transitions was treated within the so-called enthalpy approach, while a conventional nucleation-and-growth mechanistic scenario was adopted to describe the formation of reaction products. Once melting has occurred, system thermodynamics ensures the existence of driving forces for dissolution of the refractory element into the molten phase and the subsequent formation of the final solid product. The driving forces for the dissolution of the refractory element and crystallization of the product were determined in connection with the liquidus and solidus lines of the appropriate phase diagram.

By establishing a rigorous theoretical framework for the appropriate physico-chemical description of SHS processes, such a modeling approach represented, in the authors' opinion, a clean breaking point with previous attempts. Its versatility also allows consideration of, at least in principle, all different phenomena taking place during the course of the combustion reaction.

Thus, the model can be used to gain a deeper insight into the microscopic elementary phenomena involved in SHS processes through a suitable combination of experimental and modeling investigations. In particular, by means of this modeling approach, which provides a theoretical framework to relate macroscopic behavior to the microscopic scale processes, a proper interpretation of the experimental evidences can be attempted.

This, which is aimed at providing a contribution along this difficult line of inquiry, is presented in two articles. In this first article (Part I), the study focuses on the SHS reaction resulting in the formation of the TiC carbide starting from pure Ti and graphite. A generic dissolution crystallization mechanistic scenario has been adopted to simulate the formation and the microstructure of the final TiC phase. By suitably modifying the original theoretical framework proposed by Stangle and coworkers,[26] appropriate population balances have been used to simulate the microstructure evolution.

In the second article (Part II),[27] selected numerical simulation results based on the model outlined in Part I, which quantitatively describe SHS of TiC, have been illustrated and discussed in detail from the kinetic point of view. The model reliability has been also tested by comparison with suitable arranged experimental data.

It should be mentioned that the present work represents the natural evolution of previous investigations,[28,29] where, due to either the lack of experimental data or stringent space limitations, we were not able to thoroughly present, discuss, and test the proposed model.

II. MODELING OUTLINE

The mathematical model discussed in the present work is based on the modeling approach originally proposed by Stangle and co-workers at the beginning of the 1990s.[24–26] Although the general lines of approach have been left unchanged, modifications have been carried out on the theoretical framework and corresponding equations. Such modifications may be easily identified by comparing the equations reported in this work with those pertaining to Stangle and co-workers' papers. For the sake of brevity, modifications will not be here discussed in detail.

As briefly mentioned in the Introduction, the model is extremely versatile and can be, at least in principle, suitably arranged to permit the simulation of SHS processes characterized by different reaction mechanisms. However, in the present work, the attention has been focused on the cases in which a low melting point element reacts

with a refractory one to form a solid product, where the melting temperatures of both the refractory reactant and the product are higher than the maximum combustion temperature. Under such conditions, the low melting point reactant is expected to melt during the course of the SHS reaction. The melting process is accompanied by a redistribution of the melt into the porous network created by the interstices among powder particles compacted to form a pellet. As the molten phase begins to fill the accessible pores, the contact area between the reactants greatly increases thus favoring the reaction between them.

Despite its apparent simplicity, the sequence of events mentioned above involves the occurrence of a large number of complex and interconnected elementary stages. Consequently, the correct detailed description of all of them requires the development of a comprehensive, though complex, mathematical model. Such a complexity is, however, undesired for the scope of the present work, which instead is planned to focus on the basic thermodynamic and kinetic features of SHS processes. For this reason, the following, simplifying assumptions have been made: (i) the pellet of compacted powders consists of non-porous, spherical powder particles; (ii) for each solid reactant, all the powder particles have the same characteristic size; (iii) the powder mixture is isotropic with regard to all the different microstructural, physical, and chemical properties; and (iv) the combustion process is carried out under inert atmosphere or vacuum conditions.

Further aspects and assumptions of the modeling approach which deserve a detailed discussion will be dealt separately in the following subsections. For the sake of brevity, the reader is invited to refer to the Nomenclature and Appendix sections for the correct meaning of various symbols and quantities used.

A. Reaction mechanism

A porous pellet consisting of rigid spherical powder particles arranged to form a statistically disordered spatial configuration is considered. Under the assumption that each particle is basically in point contact with the nearest neighbors, it appears that the surface of contact among the powder particles has a small area. The contact surface area between the reactants increases and reaches higher values when melting of the reactant characterized by the lowest melting point occurs. In fact, the melting process is accompanied by the subsequent wetting of the solid particles.

The correct description of pore filling process by permeation of the liquid phase requires the liquid phases momentum to be suitably accounted for by means of proper momentum balance equations. However, this complicates the model beyond the scope of the present work. For this reason, this phenomenon is assumed to take place instantaneously and locally once the melt has formed.

The formation of a molten phase and the consequent wetting of the solid particles of refractory reactant have important consequences on the system reactivity. On the one hand, the existence of a molten phase induces the dissolution of the refractory reactant. On the other, it favors the occurrence of heterogeneous chemical reactions on the surface of the particles of refractory material. Under such conditions, the formation of final products during SHS processes is expected to take place by interdiffusion of solid reactants [Fig. 1(a)] or in connection with the presence of molten phase, in its bulk through dissolution-crystallization mechanism [Fig. 1(b)] or at the surface of solid particles through heterogeneous reaction [Fig. 1(c)].
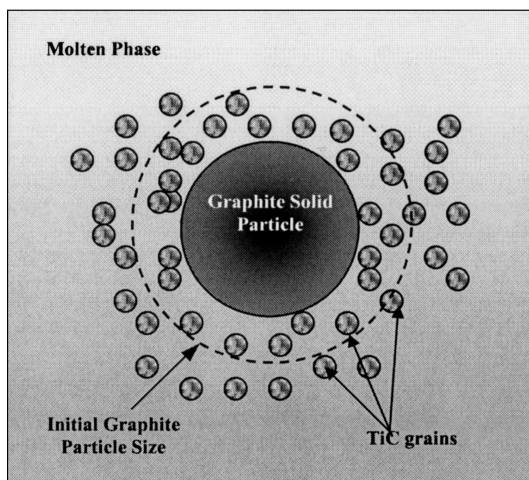
However, the reactions between solid reactants can be ruled out due to the small contact area between them and the high heating rate (i.e., the melting temperature of the low melting reactants is reached very fast), typically observed in SHS processes. These considerations reduce the number of possible mechanisms to the two involving the dissolution-crystallization mechanism and the surface reaction between a solid particle and the surrounding liquid, respectively. By observing that dissolution processes are generally faster than solid-state reactions, which require the atomistic thermal diffusion of chemical species within a solid matrix, chemical reactions at the surface of solid particles in contact with the liquid phase can be reasonably neglected. This assumption seems reasonable especially when graphite solid particles are relatively small.

Thus, under these conditions, the remaining mechanism consisting of dissolution followed by crystallization [Fig. 1(b)] appears to be the more reasonable pathway to product formation, when melting of one reactant takes place. Indeed, chemical transformations regarding solid phases very often take place via nucleation of the product phase from a parent one. The nucleation step is then followed by the growth of the nuclei which finally determines the microstructural features of product phase. In particular, nucleation-and-growth mechanisms have been observed in SHS processes where a precipitate is formed within a molten phase as a consequence of dissolution and crystallization phenomena.[30,31] Therefore, a nucleation-and-growth scenario seems to be well suited for describing the formation of the final product phase during the course of the combustion process which involves the melting of one reactant and the dissolution of the other one in the generated liquid phase.
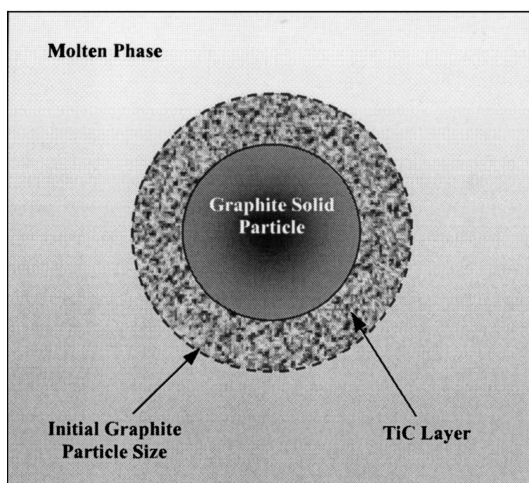
Of course, since in this latter mechanism the crystallization may involve homogeneous nucleation of the solid product within the molten phase bulk or its heterogeneous nucleation at the surface of refractory particles,
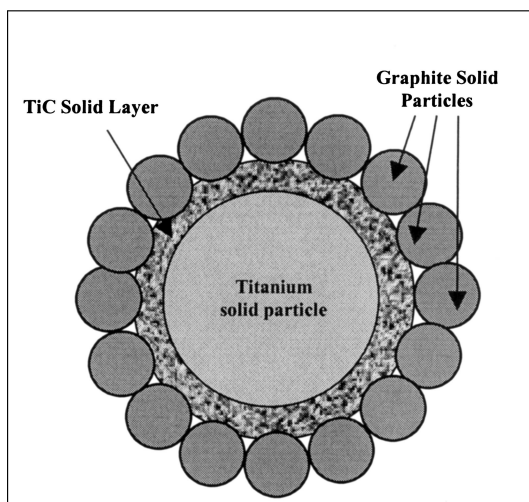
(a)

(b)

(c)

FIG. 1. Possible interactions between titanium and graphite during SHS processes: (a) solid–solid reaction, (b) dissolution and crystallization in the molten phase, and (c) solid–liquid surface reaction.

the need of a further discrimination on the possible mechanism arises.

This microscopic aspect may be clarified by comparison between proper experimental data of macroscopic quantities and the results provided by a mathematical model able to relate the system macroscopic behavior to the microscopic phenomena involved during product formation (Part II[27]).

B. Thermodynamics

The theoretical framework briefly discussed above is well suited to describing the combustion synthesis of metal carbides such as TiC, ZrC, and HfC. Indeed, SHS of metal carbides has been extensively studied, and the characteristic reactivity of metal-graphite systems has been well characterized from the experimental point of view. Whenever the above-mentioned carbides are synthesized by SHS, a relatively low melting point transition metal reacts with the refractory graphite to form the refractory carbide phase. It is worth noting that the non-stoichiometric carbide formed is also the unique product of the high-temperature reaction between the transition metal and the graphite. Thus, due to the high melting point of both the graphite and the carbide, the number of possible phases to be dealt with during the course of the numerical simulations is restricted to four. More specifically, the system reactivity determines the simultaneous presence of three solid phases, i.e., the two pure solid reactants and the final pure product and a liquid phase, basically the melt of the low melting point metal, which is able to dissolve graphite. Four is therefore the smallest possible number of phases as far as the reaction mechanism requires the presence of a molten phase.

In the present work, our attention is focused on the SHS reactivity of the Ti–C binary system. This choice is basically motivated by the largest number of papers devoted to Ti–C than to other carbide systems mentioned above.[32] It then obviously follows that all the parameters involved in the numerical simulations refer to the Ti–C system (see Part II[27]).

The system thermodynamics is accounted for by the phase diagram reported in Fig. 2.[33] It follows that Ti and C can form a single carbide TiC characterized by a non-stoichiometric composition. The existence of a stoichiometric interval, delimited by the solidus lines within which the carbide can be formed, implies possible changes in the carbide composition depending on temperature, initial stoichiometry of the Ti-C mixture and solidus lines slope. Carbide composition changes are, however, assumed to have a negligible effect on the whole combustion process. For these reasons, although we explicitly take into account the existence of the liquidus and solidus lines of the phase diagram, a stoichiometric TiC carbide is assumed to be formed whenever
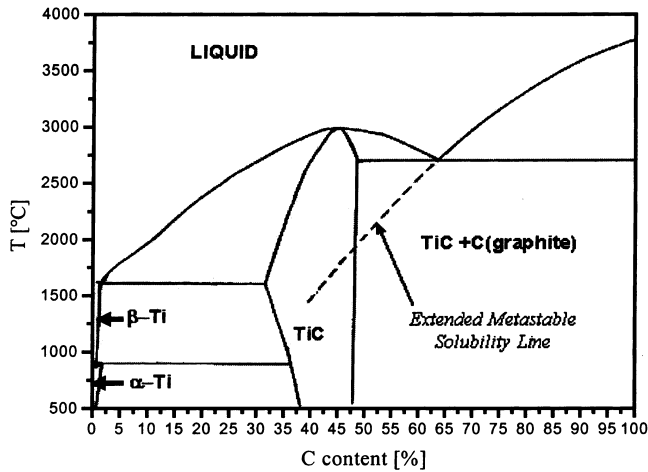
FIG. 2. Ti–C phase diagram[33] with the additional extended metastable solubility line.

thermodynamic and kinetic conditions for the formation of a solid product are satisfied.

C. Kinetic equations

On the basis of the selected reaction mechanism and the thermodynamics of the Ti–C binary system, in the following, a summary of the key equations used to describe the kinetics of TiC formation process is given.

According to the phase diagram reported in Fig. 2, when Ti melts the following driving force for graphite dissolution in the molten phase exits:

$$\Omega_D = \ln \frac{(1 - x_C)}{(1 - x_C^*)} \quad , \tag{1}$$

(refer to Appendix A for its derivation). Equilibrium concentration of C in molten Ti at a certain temperature T, x_C^*, is determined by the C liquidus line in the phase diagram (i.e., the solubility of C in liquid Ti), whose metastable extension below the solidification line is explicitly reported in the phase diagram.

The dissolution of C in the molten phase can be described according to the following mass balance equation for solid C and the corresponding initial conditions:

$$\frac{\partial m_C^{(s)}}{\partial t} = -a_{C \to liq} N_{C \to liq} \quad , \tag{2}$$

$$t = 0 \quad m_C^{(s)} = m_C^0 \quad , \tag{3}$$

where $a_{C \to liq}$ represents the surface area density of solid C in contact with the molten phase, and $N_{C \to liq}$ represents the mass flux of C dissolving in the molten phase (the reader should refer to Appendix A and B for more details). The latter is given by

$$N_{C \to liq} = \frac{2M_C \left(\dfrac{m_{Ti}^{(liq)}}{M_{Ti}} + \dfrac{m_C^{(liq)}}{M_C} \right) D_{B \to liq} \Omega_D}{\phi^{(liq)} d_{PC}} \quad , \tag{4}$$

where $D_{B \to liq}$ represents the diffusivity of graphite in the liquid phase. It is worth noting that this latter parameter has been identified with the diffusivity of graphite in molten titanium under the assumption of negligible concentration effect on the diffusivity.

As a result of the dissolution process, the C content, x_C, in the molten phase increases. When, due to the dissolution process, x_C reaches, at a certain temperature T, the region of the phase diagram between the TiC liquidus and solidus lines, the melt becomes supersaturated. Under this condition, crystallization of TiC final product starts. More specifically, stable crystalline nuclei are formed at suitable nucleation sites, replacing pre-existing unstable germs of precipitation. Depending on the occurrence of homogeneous or heterogeneous nucleation phenomena, the nucleation sites are statistically distributed, respectively, in the bulk of the molten phase or at the surface of the solid particles. Then, once a stable TiC nucleus has been formed, it will consequently grow.

It is worth noting that the simultaneous occurrence of graphite dissolution and TiC crystallization induces a competition between them with regard to the C content x_C in the molten phase. Actually, such a competition univocally determines C content in the melt as a result of a dynamical equilibrium. In fact, as the C content overcomes the thermodynamic equilibrium threshold represented by the liquidus line, crystallization occurs to restore the C concentration at the thermodynamic equilibrium under the action of two driving forces, namely:

$$\Omega_N = \ln \left(\frac{x_C}{x_C^{(liquidus)}} \right) \quad , \tag{5}$$

and

$$\Omega_G = \frac{x_C - x_C^{(liquidus)}}{x_C^{(solidus)} - x_C^{(liquidus)}} \quad , \tag{6}$$

for nucleation[34] and growth,[26] respectively. The exact position of the dynamical equilibrium is determined by the relative rates of dissolution and nucleation-growth processes.

The nucleation rate J_n can be expressed by the following equation[34]

$$J_n = B_0 \frac{T \rho_{Ti}^{(liq)}}{M_{Ti}} \exp \left(-\frac{E_N + E_D}{RT} \right) \quad , \tag{7}$$

which quantifies the rate at which nuclei are formed. The nucleation activation energy E_N is given by

$$E_N = \frac{4}{3} \pi \gamma (r^*)^2 N_A \quad , \quad (8)$$

where the critical radius is expressed as

$$r^* = \frac{2\gamma M_{TiC}}{RT \rho_{TiC}^{(s)} \Omega_N} \quad . \quad (9)$$

Under the assumption that the grains maintain a spherical shape during the course of the growth process, the grain growth rate G_r can be expressed by the following equation[26]

$$G_r = \frac{\Omega_G D_{B \to liq}}{r} \quad . \quad (10)$$

By neglecting death terms, the formation of nuclei of product phase as well as the growth of original nuclei into grains of increasing size can be dealt with by means of the population balance given below[35,36]

$$\frac{\partial n}{\partial t} = -\frac{\partial}{\partial r} (G_r n) + \delta_{Dirac} (r - r^*) J_n \quad , \quad (11)$$

$$t = 0 \quad \forall r \quad n = 0 \quad , \quad (12)$$

$$r = 0 \quad \forall t > 0 \quad \frac{\partial n}{\partial r} = 0 \quad . \quad (13)$$

Following the approach adopted by Hulburt and Katz,[37] nucleation at r^* has been directly included in the population balance [Eq. (11)] by means of a Dirac delta function. The initial condition represents the complete absence of any class (i.e., size) of grains before nucleation begins, while Eq. (13) represents the no-growth condition from zero size grains.

The assumption that single grains grow according to a spherical symmetry can be regarded as satisfactory as far as the grains have a relatively small size, i.e., during the first stages of the growth process. The validity of such an assumption certainly breaks down when the total volume fraction occupied by grains increases. Under such conditions, indeed, the single grains may impinge on each other and, correspondingly, meet obstacles to their spherical growth. To properly take into account this possible steric hindrance, an accurate description of the so-called "hard impingement" process[38] should be included in the model. However, since the actual importance of this phenomenon within a porous system required further investigation, such a process will be discussed in a future paper.

In the present work, so-called "soft impingement,"[38] which greatly simplifies the model equations and the numerical computations, is instead adopted. Correspondingly, the forms of Eq. (10) and the related boundary conditions do not take into account any mechanism that could explicitly limit the growth process or could affect the geometry of growing particles. Therefore, the only

limitation to the growth of the spherically symmetrical, non-interacting grains is given by the total occupation of the available volume.

D. Energy balance

Under the assumption that no change in the pellet volume occurs during the SHS process, the energy balance is represented by the following equation and the corresponding initial and boundary conditions:

$$\frac{\partial H_{mix}}{\partial t} = -\frac{\partial}{\partial z}\left(-k_{mix}\frac{\partial T}{\partial z}\right) - \frac{4h}{D}(T - T_0)$$
$$- \frac{4\sigma \epsilon_{mix}}{D}(T^4 - T_0^4) \quad , \quad (14)$$

$$t = 0 \quad \forall z \quad H_{mix} = H_{mix}^0 \quad , \quad (15)$$

$$z = 0 \quad \forall t > 0$$

$$\begin{cases} -k_{mix}\dfrac{\partial T}{\partial z} = q_{ig}(t) & \text{if } t \leq t_{ig} \\[2mm] -k_{mix}\dfrac{\partial T}{\partial z} = -h(T - T_0) & \text{if } t > t_{ig} \\[2mm] \qquad\qquad - \sigma\epsilon_{mix}(T^4 - T_0^4) \end{cases} , \quad (16)$$

$$z = L \quad \forall t > 0 \quad -k_{mix}\frac{\partial T}{\partial z} = h(T - T_0)$$
$$+ \sigma\epsilon_{mix}(T^4 - T_0^4) \quad . \quad (17)$$

The term on the left hand side of Eq. (14) represents the accumulation of the total enthalpy density H_{mix}. The terms on the right hand side account for the heat transfer by thermal conduction within the sample, the heat transfer by natural conduction and the heat transfer to the surrounding by radiation, respectively. The function $q_{ig}(t)$ appearing in the boundary condition of Eq. (16) represents the simulated ignition flux at one end of the pellet. Refer to Appendix C and D for more details about the quantities q_{ig}, k_{mix}, and ϵ_{mix}.

E. Phase transitions

Any change in the enthalpy content H_{mix} determines a corresponding change in the local temperature and, whenever thermodynamic conditions are satisfied, the occurrence of phase transitions. Such changes as well as their interconnection with temperature and system composition are accounted for through the so-called enthalpy approach.[18,39]

The enthalpy approach must be regarded as the reference theoretical framework to deal with the possible phase transitions during the ignition and the propagation of the combustion wave. It represents the relationships between enthalpy content, temperature and composition

of the mixture as illustrated by the equations reported in Table I. In particular, given H_{mix} and system composition, this relationship allows evaluation of the system temperature or the fraction of the species undergoing phase transition. The total (i.e., solid + liquid) mass concentrations of reactants, products, and diluent have been calculated from the materials balances reported in the next section.

It is worth noting that, following this approach, the reaction enthalpy is implicitly taken into account. For this reason, it does not appear in the right hand side of the energy balance.

F. Material balances

In principle, material balances must take into account macroscopic mass transport phenomena due to the relative motion of the different phases, such as phase separation, capillary spreading, and particle buoyancy. The description of such phenomena would require the formulation of momentum continuity equations coupled with

the energy and mass balances, since macroscopic flows of both solid and liquid phases contribute to the energy and mass conservation.

To simplify model calculations, we assumed that macroscopic flows of solid and liquid phases are negligible. Correspondingly, no momentum continuity equation has been included in the model and material balance equations can be expressed in a simple algebraic form.

The transformation of the reactants Ti and C into the final carbide TiC is taken into account by means of the following material balance equations:

$$m_{Ti} + \frac{M_{Ti}}{M_{TiC}} m_{TiC} = m_{Ti}^0 \quad , \tag{18}$$

$$m_C + \frac{M_C}{M_{TiC}} m_{TiC} = m_C^0 \quad , \tag{19}$$

$$m_{TiC} = m_{TiC}^0 + \frac{4}{3} \pi \rho_{TiC} \int_0^\infty r^3 n(r) dr \quad , \tag{20}$$

TABLE I. Enthalpy expressions corresponding to the adopted approach.

Enthalpy range	H_{mix}, T relationship	H_{mix}, $m_{Ti}^{(liq)}$ relationship
$H_{0,mix} \leqslant H_{mix} < H_{1,mix}$	$H_{mix} = H_{0,mix} + m_{Ti}\int_{T_0}^{T} C_{pTi}^{(\alpha)}(T)dT + m_C\int_{T_0}^{T} C_{PC}(T)dT + m_{TiC}\int_{T_0}^{T} C_{pTiC}(T)dT$ $+ m_{Diluent}\int_{T_0}^{T} C_{pDiluent}(T)dT + m^{(gas)}\int_{T_0}^{T} C_p^{(gas)}(T)dT$	$m_{Ti}^{(liq)} = 0$
$H_{1,mix} \leqslant H_{mix} \leqslant H_{2,mix}$	$T = T_{t,Ti}$	$m_{Ti}^{(liq)} = 0$
$H_{2,mix} < H_{mix} < H_{3,mix}$	$H_{mix} = H_{2,mix} + m_{Ti}\int_{T_{t,Ti}}^{T} Cp_{Ti}^{(\beta)}(T)dT + m_C\int_{T_{t,Ti}}^{T} Cp_C(T)dT + m_{TiC}\int_{T_{t,Ti}}^{T} Cp_{TiC}(T)dT$ $+ m_{Diluent}\int_{T_{t,Ti}}^{T} Cp_{Diluent}(T)dT + m^{(gas)}\int_{T_{t,Ti}}^{T} Cp^{(gas)}(T)dT$	$m_{Ti}^{(liq)} = 0$
$H_{3,mix} \leqslant H_{mix} \leqslant H_{4,mix}$	$T = T_{m,Ti}$	$m_{Ti}^{(liq)} = \dfrac{H_{mix} - H_{3,mix}}{\lambda_{m,Ti}}$
$H_{4,mix} < H_{mix}$	$H_{mix} = H_{4,mix} + m_{Ti}\int_{T_{m,Ti}}^{T} Cp_{Ti}^{(liq)}(T)dT + m_C\int_{T_{m,Ti}}^{T} Cp_C(T)dT + m_{TiC}\int_{T_{m,Ti}}^{T} Cp_{TiC}(T)dT$ $+ m_{Diluent}\int_{T_{m,Ti}}^{T} Cp_{Diluent}(T)dT + m^{(gas)}\int_{T_{m,Ti}}^{T} Cp^{(gas)}(T)dT$	$m_{Ti}^{(liq)} = m_{Ti}$

$H_{0,mix} = m_{Ti}H_{Ti}^0 + m_C H_C^0 + m_{TiC}H_{TiC}^0 + m_{Diluent}H_{Diluent}^0 + m^{(gas)}H^{(gas),0}$

$H_{1,mix} = H_{0,mix} + m_{Ti}\int_{T_0}^{T_{t,Ti}} Cp_{Ti}^{(\alpha)}(T)dT + m_C\int_{T_0}^{T_{t,Ti}} Cp_C(T)dT + m_{TiC}\int_{T_0}^{T_{t,Ti}} Cp_{TiC}(T)dT + m_{Diluent}\int_{T_0}^{T_{t,Ti}} Cp_{Diluent}(T)dT + m^{(gas)}\int_{T_0}^{T_{t,Ti}} Cp^{(gas)}(T)dT$

$H_{2,mix} = H_{1,mix} + m_{Ti}\lambda_{t,Ti}$

$H_{3,mix} = H_{2,mix} + m_{Ti}\int_{T_{t,Ti}}^{T_{m,Ti}} Cp_{Ti}^{(\beta)}(T)dT + m_C\int_{T_{t,Ti}}^{T_{m,Ti}} Cp_C(T)dT + m_{TiC}\int_{T_{t,Ti}}^{T_{m,Ti}} Cp_{TiC}(T)dT + m_{Diluent}\int_{T_{t,Ti}}^{T_{m,Ti}} Cp_{Diluent}(T)dT + m^{(gas)}\int_{T_{t,Ti}}^{T_{m,Ti}} Cp^{(gas)}(T)dT$

$H_{4,mix} = H_{3,mix} + m_{Ti}\lambda_{m,Ti}$

$$m_{\text{Diluent}} = m_{\text{Diluent}}^0 \quad , \tag{21}$$

$$m^{(\text{gas})} = \frac{M^{(\text{gas})}P}{RT} \quad . \tag{22}$$

According to the general laws of mass conservation, the relative distribution of the reactants in the different solid and liquid phases is given by the following equations:

$$m_{\text{Ti}}^{(\text{s})} + m_{\text{Ti}}^{(\text{liq})} = m_{\text{Ti}} \quad , \tag{23}$$

$$m_{\text{C}}^{(\text{s})} + m_{\text{C}}^{(\text{liq})} = m_{\text{C}} \quad , \tag{24}$$

$$m_{\text{TiC}}^{(\text{s})} = m_{\text{TiC}} \quad , \tag{25}$$

$$m_{\text{Diluent}}^{(\text{s})} = m_{\text{Diluent}} \quad , \tag{26}$$

while the total amount of each phase is easily obtained as follows:

$$m_{\text{Ti}}^{(\text{s})} + m_{\text{C}}^{(\text{s})} + m_{\text{TiC}}^{(\text{s})} + m_{\text{Diluent}}^{(\text{s})} = m^{(\text{s})} \quad , \tag{27}$$

$$m_{\text{Ti}}^{(\text{liq})} + m_{\text{C}}^{(\text{liq})} = m^{(\text{liq})} \quad . \tag{28}$$

III. CONCLUSION

A novel mathematical model to simulate SHS processes was proposed in this paper. All the relevant physical and chemical processes that take place during reaction evolution were modeled through appropriate mass and energy balances, which constitute a set of nonlinear and interrelated partial differential and algebraic equations. Microstructural evolution has been simulated by means of suitable population balances and properly evaluating the different driving forces from the relevant phase diagram. In particular, the occurrence of phase transitions was treated within the so-called enthalpy approach, while a conventional nucleation-and-growth mechanistic scenario was adopted to describe the formation of reaction products.

The theoretical approach provides a fundamental understanding of combustion synthesis processes, thus overcoming, at least partially, the well-known limitations associated with the representation of SHS phenomenology in terms of homogeneous or pseudo-homogeneous processes.

NOMENCLATURE

B_0	pre-exponential factor of nucleation ($\text{m}^{-3}\text{s}^{-1}$)
C_{p}	heat capacity ($\text{J kg}^{-1} \text{K}^{-1}$)
d_{p}	particle diameter (m)
D	pellet diameter (m)
E_{D}	activation energy for graphite diffusion in liquid Ti (J mol^{-1})
h	heat-transfer coefficient for natural convection ($\text{J s}^{-1} \text{m}^{-2} \text{K}^{-1}$)
H	enthalpy density (J m^{-3})
k	thermal conductivity ($\text{W m}^{-1} \text{K}^{-1}$)
l_{pore}	pore size (m)
$l_{\text{pore}}^{\text{av}}$	average pore size (m)
l_{pore}^0	minimum pore size (m)
l_{pore}^*	largest radius of all pores filled with liquid (m)
L	pellet length (m)
m	mass concentration (kg m^{-3})
M	molecular weight (kg mol^{-1})
n	grain density (m^{-4})
N_{A}	Avogadro's number (mol^{-1})
P	gas pressure (Pa)
r	grain size (m)
r^*	critical grain size (m)
R	universal gas constant ($\text{J mol}^{-1} \text{K}^{-1}$)
R_0	internal electric resistance of ignition energy supply circuit (ohm)
t	time (s)
t_{ig}	ignition time (s)
T	temperature (K)
T_0	initial temperature (K)
x_{C}	molar fraction of graphite in liquid phase $\left(= \left[1 + \frac{M_{\text{C}}}{M_{\text{Ti}}} \frac{m_{\text{Ti}}^{(\text{liq})}}{m_{\text{C}}^{(\text{liq})}} \right]^{-1} \right);$
$x_{\text{C}}^{(\text{liq})}$	molar fraction of graphite on TiC liquidus line
$x_{\text{C}}^{(\text{sol})}$	molar fraction of graphite on TiC solidus line
x_{C}^*	solubility of graphite in liquid Ti
V_0	imposed voltage to ignition energy supply (V)
z	axial position (m)

Greek letters

δ_{Dirac}	Dirac delta function
ϵ	emissivity
ϕ	volumetric fraction
γ	interfacial energy between liquid Ti and solid TiC (J m^{-2})
λ	latent heat of transition phase (J mol^{-1})
ρ	density (kg m^{-3})
σ	Stefan–Boltzmann's constant ($\text{W m}^{-2} \text{K}^{-4}$)
ζ	electrical resistivity (ohm m)

Subscripts

C	graphite
Diluent	inert phase in the initial reacting mixture
m	melting
mix	mixture
t	α–β phase transition
Ti	titanium

TiC   titanium carbide
W   tungsten

Superscripts

(α)   low-temperature solid-phase of reactant Ti
(β)   high-temperature solid-phase of reactant Ti
(fluid)   fluid phase (gas + liquid)
(gas)   gas phase
(liq)   liquid phase
(s)   solid phase
0   initial or reference value

REFERENCES

1. F. Booth: The theory of self-propagating exothermic reactions in solid systems. *Trans. Faraday Soc.* **49,** 272 (1953).

2. J.D. Walton and N.E. Poulos: Cermets from thermite reactions. *J. Am. Ceram. Soc.* **42,** 40 (1959).

3. A.G. Merzhanov and I.P. Borovinskaya: Self-propagating high-temperature synthesis of refractory inorganic compounds. *Dokl. Akad. Nauk SSSR* **204,** 366 (1972).

4. A. Varma, A.S. Rogachev, A.S. Mukasyan, and S. Hwang: Combustion synthesis of advanced materials: Principles and applications. *Adv. Chem. Eng.* **24,** 79 (1998).

5. J.J. Moore and H.J. Feng: Combustion synthesis of Advanced Materials: Part I. Reaction parameters. *Prog. Mater. Sci.* **39,** 243 (1995).

6. J.J. Moore and H.J. Feng: Combustion synthesis of Advanced Materials: Part II. Classification, application and modeling. *Prog. Mater. Sci.* **39,** 275 (1995).

7. B.V. Novozhilov: The rate of propagation of the front of an exothermic reaction in a condensed phase. *Dokl. Akad. Nauk SSSR.* **141,** 151 (1961).

8. B.I. Khaikin and A.G. Merzhanov: Theory of thermal propagation of a chemical reaction front. *Fiz. Goreniya Vzryva.* **2**(3), 36 (1966).

9. A.G. Merzhanov: New elementary model of the second kind. *Dokl. Akad. Nauk SSSR* **233**(6), 1130 (1977).

10. S.B. Margolis: An asymptotic theory of condensed two-phase flame propagation. *SIAM J. Appl. Math.* **43,** 351 (1983).

11. G. Cao and A. Varma: A new expression for velocity of the combustion front during self-propagating high-temperature synthesis. *Combust. Sci. Technol.* **102,** 181 (1994).

12. G.M. Makhviladze and B.V. Novozilov: Two-dimensional stability of combustion of condensed systems. *Zh. Prikl. Mekh. I Tekhn. Fiz.* **5,** 51 (1971).

13. K.G. Shkadinskii, B.I. Khaikin, and A.G. Merzhanov: Propagation of a pulsating exothermic reaction front in the condensed phase. *Fiz. Goreniya Vzryva.* **8,** 202 (1971).

14. A.P. Aldushin, V.D. Lugovoi, A.G. Merzhanov, and B.I. Khaikin: Conditions of stationary combustion wave degradation. *Dokl. Akad. Nauk SSSR* **243,** 1434 (1978).

15. B.J. Matkowsky and G.L. Sivanshinsky: Propagation of a pulsating reaction front in solid fuel combustion. *SIAM J. Appl. Math.* **35,** 465 (1978).

16. J.A. Puszynski, J. Degreve, and V. Hlavacek: Modeling of exothermic solid-solid noncatalytic reactions. *Ind. Eng. Chem. Res.* **26,** 1424 (1987).

17. A.M. Kanury: A kinetic model for metal + nonmetal reactions. *Metall. Trans.* **23A,** 2349 (1992).

18. A.K. Bhattacharya: Temperature enthalpy approach to the modeling of self-propagating combustion synthesis of materials. *J. Mater. Sci.* **27**(11), 3050 (1992).

19. A.S. Astapchik, E.P. Podvoisky, I.S. Chebotko, B.M. Khusid, A.G. Merzhanov, and B.B. Khina: Stochastic model for wavelike isothermal reaction in condensed heterogeneous systems. *Phys. Rev. E* **47**(1), 319 (1993).

20. S. Hwang, A.S. Mukasyan, A.S. Rogachev, and A. Varma: Combustion wave microstructure in gas-solid system: Experiments and theory. *Combust. Sci. Technol.* **123,** 165 (1997).

21. E.A. Nekrasov, Y.M. Maksimov, and A.P. Aldushin: Mathematical model of combustion of a titanium-carbon system. *Fiz. Goreniya Vzryva.* **17**(5), 39 (1981).

22. A. Makino: Fundamental aspects of the heterogeneous flame in the self-propagating high-temperature synthesis (SHS) process. *Prog. Energy Combust. Sci.* **27**(1), 1 (2001).

23. V.I. Yukhvid, S.V. Makladov, P.V. Zhirkov, V.A. Gorshkov, N.I. Timokhin, and A.Y. Dovzhenko: Combustion synthesis and structure formation in a model Cr–CrO$_3$ self-propagating high-temperature synthesis system. *J. Mater. Sci.* **32,** 1915 (1997).

24. Y. Zhang and G.C. Stangle: A micromechanistic model of the combustion synthesis process: Part I. Theoretical development. *J. Mater. Res.* **9,** 2582 (1994).

25. Y. Zhang and G.C. Stangle: A micromechanistic model of the combustion synthesis process: Part II. Numerical simulation. *J. Mater. Res.* **9,** 2605 (1994).

26. Y. Zhang and G.C. Stangle: A micromechanistic model of microstructure development during the combustion synthesis process. *J. Mater. Res.* **10,** 962 (1995).

27. A.M. Locci, A. Cincotti, F. Delogu, R. Orrù, and G. Cao: Combustion synthesis of metal carbides: Part II. Numerical simulation and comparison with experimental data. *J. Mater. Res.* **20,** 1269 (2005).

28. A.M. Locci, A. Cincotti, F. Delogu, R. Orrù, and G. Cao: Modeling of Self-propagating reaction: past approaches and future directions. *Int. J. of SHS* **12,** 61 (2003).

29. A.M. Locci, A. Cincotti, F. Delogu, R. Orrù, and G. Cao: Advanced modeling of self-propagating high-temperature synthesis: the case of the Ti–C system. *Chem. Eng. Sci.* **59,** 5121 (2004).

30. H. Fan, H. Chai, and Z. Jin: Dual-solution precipitation mechanism of combustion synthesis of TiC-Fe cermet with finer Ti powder. *J. Mater. Sci.* **36,** 5559 (2001).

31. H. Fan, H. Chai, and Z. Jin: Dissolution-precipitation mechanism of self-propagating high-temperature synthesis of mononickel aluminide. *Intermetallics* **9,** 609 (2001).

32. J.B. Holt and Z.A. Munir: Combustion synthesis of titanium carbide: Theory and experiment. *J. Mater. Sci.* **21,** 251 (1986).

33. *Binary Phase Diagrams,* edited by T.B. Massalski (American Society for Metals, Metals Park, OH, 1986).

34. J.A. Dirksen and T.A. Ring: Fundamental of crystallization: Kinetic effects on particle size distributions and morphology. *Chem. Eng. Sci.* **46,** 2389 (1991).

35. A.D. Randolph and M.A. Larson: *Theory of Particulate Process: Analysis and Techniques of Continuous Crystallization,* 2nd ed. (Academic Press, San Diego, CA, 1988).

36. D. Ramkrishna: *Population Balances, Theory and Application to Particulate System in Engineering* (Academic Press, London, U.K., 2000).

37. H.M. Hulburt and S. Katz: Some problem in particle technology: A statistical mechanical formulation. *Chem. Eng. Sci.* **19,** 555 (1964).

38. M.T. Clavaguera-Mora, N. Clavaguera, D. Crespo, and T. Pradell: Crystallization kinetics and microstructure development in metallic systems. *Prog. Mater. Sci.* **47,** 559 (2002).

39. J.E. Gatica, P.A. Dimitriou, J.A. Puszynski, and V. Hlavacek:

Melting effects on reaction front propagation in gasless combustion. *Int. J. SHS* **4,** 123 (1995).

40. R.B. Bird, W.E. Stewart, and E.N. Lightfoot: *Transport Phenomena* (Wiley, New York, NY, 1960).
41. F.A.L. Dullien: *Porous Media: Fluid Transport and Pore Structure,* 2nd ed. (Academic Press Inc., San Diego, CA, 1992).
42. J. Szekely and N.J. Themelis: *Rate Phenomena in Process Metallurgy* (John Wiley & Sons, New York, NY, 1971).
43. A.V. Luikov, A.G. Shashkov, L.L. Vasiliev, and Y.E. Fraiman: Thermal conductivity of porous systems. *Int. J. Heat Mass Transf.* **11,** 117 (1968).
44. C.T. Hsu, P. Cheng, and K.W. Wong: Modified Zehner–Schlunder models for stagnant thermal conductivity of porous media. *Int. J. Heat Mass Transf.* **37,** 2751 (1994).
45. B.P. Singh and M. Kaviany: Effect of solid conductivity on radiative heat transfer in packed beds. *Int. J. Heat Mass Transfer.* **37,** 2579 (1994).

APPENDIX

A. Dissolution flux

The mass flux of C dissolving in the molten phase $N_{C\rightarrow liq}$, can be evaluated through the following equation, which has been developed for the pseudo-stationary diffusion problem of a spherical particle of $C^{(s)}$ into a stagnant liquid phase[40]:

$$\frac{\partial}{\partial \xi}\left(\xi^2 N_{C\rightarrow liq}\right) = 0 \quad , \tag{A1}$$

where ξ is the radial coordinate along the diffusion direction. By solving Eq. (A1) along with the following boundary conditions:

$$\xi = \frac{d_{p_C}}{2} \quad x_C = x_C^* \quad , \tag{A2}$$

$$\xi \rightarrow \infty \quad x_C = x_C(t) \quad , \tag{A3}$$

$N_{C\rightarrow liq}$ expressed by Eq. (4) has been obtained.

B. Contact surface area between solid C particle and molten phase

The surface area density $a_{C\rightarrow liq}$ affected by the wetting phenomena corresponds to the portion of total $C^{(s)}$ particle surface in contact with the molten phase. Such a quantity can be easily obtained by summing up surface areas of single $C^{(s)}$ particles, as follows:

$$a_{C\rightarrow liq} = a_{frac} \frac{6}{d_{p_C}^0} \sqrt[3]{\phi_C^{(s),0}(\phi_C^{(s)})^2} \tag{A4}$$

where a_{frac} represents the fraction of the total surface of the $C^{(s)}$ particles in contact with the molten phase. This quantity depends on the statistical distribution of pore sizes determined by the approximately random packing of spherical particles.

Under the assumption that the pore-size distribution can be described by a Rayleigh-type one and that the

molten phase fills the pores starting from the smallest ones, the quantity a_{frac} can be evaluated according to the following equation[41]:

$$a_{frac} = \frac{\int_{l_{pore}^0}^{l_{pore}^*} \left\{ l_{pore}\left[\frac{l_{pore} - l_{pore}^0}{(l_{pore}^{av} - l_{pore}^0)^2}\right] \exp\left[-\frac{1}{2}\left(\frac{l_{pore} - l_{pore}^0}{l_{pore}^{av} - l_{pore}^0}\right)^2\right]\right\} dl_{pore}}{\int_{l_{pore}^0}^{\infty} \left\{ l_{pore}\left[\frac{l_{pore} - l_{pore}^0}{(l_{pore}^{av} - l_{pore}^0)^2}\right] \exp\left[-\frac{1}{2}\left(\frac{l_{pore} - l_{pore}^0}{l_{pore}^{av} - l_{pore}^0}\right)^2\right]\right\} dl_{pore}} \quad . \tag{A5}$$

Here, the upper endpoint of the integral at numerator, l_{pore}^* represents the largest radius belonging to the subset of pores filled with molten phase.[41] It can be shown that l_{pore}^* is indirectly connected with the liquid $\phi^{(liq)}$ and solid $\phi^{(s)}$ volume fractions through the following equation[41]:

$$\frac{\phi^{(liq)}}{1 - \phi^{(s)}} = \frac{\int_{l_{pore}^0}^{l_{pore}^*} \left\{ l_{pore}^2\left[\frac{l_{pore} - l_{pore}^0}{(l_{pore}^{av} - l_{pore}^0)^2}\right] \exp\left[-\frac{1}{2}\left(\frac{l_{pore} - l_{pore}^0}{l_{pore}^{av} - l_{pore}^0}\right)^2\right]\right\} dl_{pore}}{\int_{l_{pore}^0}^{\infty} \left\{ l_{pore}^2\left[\frac{l_{pore} - l_{pore}^0}{(l_{pore}^{av} - l_{pore}^0)^2}\right] \exp\left[-\frac{1}{2}\left(\frac{l_{pore} - l_{pore}^0}{l_{pore}^{av} - l_{pore}^0}\right)^2\right]\right\} dl_{pore}} \quad . \tag{A6}$$

where l_{pore}^{av} has been evaluated by using the concept of hydraulic radius[40]:

$$l_{pore}^{av} = \frac{d_{p_{mix}}}{6}\left(\frac{1 - \phi^{(s)} - \phi^{(liq)}}{\phi^{(s)} + \phi^{(liq)}}\right) \quad . \tag{A7}$$

The average particle diameter d_{pmix}, appearing in Eq. (A7) has been calculated by means of the following mixing rules:

$$d_{p_{mix}} = \sum_i \left(\frac{\phi_i^{(s)}}{d_{pi}^2}\right) \Big/ \sum_i \left(\frac{\phi_i^{(s)}}{d_{pi}^3}\right) \quad , \tag{A8}$$

where

$$d_{p_i} = d_{pi}^0 \sqrt[3]{m_i^{(s)}/m_i^0} \quad , \tag{A9}$$

if i = Ti, C, or Diluent, while the average particle diameter of the final product is given by

$$
d_{pTiC} = \left[2\int_0^\infty rn(r)\mathrm{d}r + \frac{\phi_C^0}{\frac{\pi}{6}(d_{pTiC}^0)^2} \right] \Bigg/ \left[\int_0^\infty n(r)\mathrm{d}r + \frac{\phi_C^0}{\frac{\pi}{6}(d_{pTiC}^0)^3} \right] . \tag{A10}
$$

In particular, this last equation takes into account the TiC formed by crystallization as well as the TiC added to the initial mixture as diluent.

C. Ignition flux

Ignition flux q_{ig}, appearing in the boundary condition [Eq. (16)] can be expressed as

$$
q_{ig} = \left(\frac{d_{coil}}{d}\right)^2 \sigma F(T_{coil}^4 - T^4) \quad, \tag{A11}
$$

where d_{coil} is the diameter of the tungsten coil used as ignition source as specified in the Sec. II, and F the view factor between the coil and the ignition surface of the pellet;[42] q_{ig} represents the heat flux provided by the tungsten coil to the pellet surface.

The temperature of the tungsten coil T_{coil} can be obtained by the following energy balance:

$$
\rho_W Cp_W \frac{\partial T_{coil}}{\partial t} = \frac{\zeta_W}{s_{coil}^2 \left(R_0 + \zeta_W \frac{L_{coil}}{s_{coil}}\right)^2} V_0^2
$$
$$
- \left(\frac{4}{d_{coil}} + \frac{2}{L_{coil}}\right)
$$
$$
[h(T_{coil} - T_0) + \sigma\epsilon_W(T_{coil}^4 - T_0^4)] \quad, \tag{A12}
$$

along with the initial condition

$$
t = 0 \quad T_{coil} = T_0 \quad, \tag{A13}
$$

where the terms of the right hand side represents the heat generation by Joule effect and the heat loss by natural convection and thermal radiation, respectively. In particular, the coil has been modeled as a disk of diameter d_{coil} and height h_{coil} when simulating the heat transfer to the pellet and the surroundings, while a wire shape of length L_{coil} and cross section s_{coil} has been assumed regarding the heat generation by Joule effect.

It worth noting that Eq. (A12) has been validated by comparing model results to experimental data of T_{coil} measured by a pyrometer at different values of V_0. Parameters needed for solving Eqs. (A11) and (A12) are reported in Table II of the companion paper.[27]

D. Thermal conductivity and emissivity of the mixture

The physical and chemical changes taking place during the course of the combustion process as well as the existence of an extended porous structure strongly affect heat transfer phenomena. However, it is worth noting that the heat-transfer processes due to natural convection into the liquid and gaseous phases can be neglected when the pore size is lower than about 1 mm.[43] It then follows that only thermal conduction and radiation processes contribute to the effective thermal conductivity k_{mix} which appears in Eq. (14). The two contributions k_{mix}^C and k_{mix}^R to the effective thermal conductivity k_{mix}, connected with the heat conduction and radiation processes respectively, can be suitably evaluated according to the following expressions:

$$
k_{mix} = k_{mix}^C + k_{mix}^R \quad. \tag{A14}
$$

The quantity k_{mix}^C has been calculated by means of the modified Zehner and Schlunder's approach proposed by Hsu et al.[44] In particular, an expression to evaluate the so-called stagnant thermal conductivity of a packed-sphere finite contact area among the spherical particles was proposed. The equation worked out to quantify k_{mix}^C is the following one:

$$
k_{mix}^C = k^{(fluid)}\left(1 - \sqrt{1 - \phi^{(gas)}}\right)
$$
$$
+ \frac{\sqrt{1 - \phi^{(gas)}}}{\Lambda}\left(1 - \frac{1}{(1 + ab\psi^c)^2}\right)
$$
$$
+ \frac{2\sqrt{(1 - \phi^{(gas)})}}{[1 - \Lambda b\psi^c + (1 - \Lambda)ab\psi^c]}
$$
$$
\left\{\left(\frac{(1 - \Lambda)(1 + a)b\psi^c}{[1 - \Lambda b\psi^c + (1 - \Lambda)ab\psi^c]^2}\right)\right.
$$
$$
\ln\left(\frac{1 + ab\psi^c}{(1 + a)\Lambda b\psi^c}\right) - \frac{1 + b\psi^c + 2ab\psi^c}{2(1 + ab\psi^c)^2}
$$
$$
\left. - \frac{(b\psi^c - 1)}{[1 - \Lambda b\psi^c + (1 - \Lambda)ab\psi^c](1 + ab\psi^c)}\right\} , \tag{A15}
$$

where $\Psi = \phi^{(gas)}/1 - \phi^{(gas)}$ and $\Lambda = k^{(fluid)}/k^{(s)}$. The numerical values of a, b, and c reported in the cited reference has been used.

In order to evaluate the average thermal conductivities of the different phases involved in the process, the following mixing rules have been adopted:

$$
k^{(fluid)} = \frac{\phi^{(gas)}k^{(gas)} + \phi^{(liq)}k^{(liq)}}{\phi^{(gas)} + \phi^{(liq)}} \quad, \tag{A16}
$$

$$k^{(\text{liq})} = \sum_i (\phi_i^{(\text{liq})} k_i^{(\text{liq})} / \phi^{(\text{liq})}) \quad i = \text{Ti,C} \quad , \tag{A17}$$

$$k^{(\text{s})} = \sum_i (\phi_i^{(\text{s})} k_i^{(\text{s})} / \phi^{(\text{s})}) \quad i = \text{Ti, C, TiC, Diluent} \quad , \tag{A18}$$

The contribution $k_{\text{mix}}^{\text{R}}$ related to the radiation process is instead evaluated by using the equation originally employed to quantify the radiant conductivity of a packed bed formed by opaque spherical particles:[45]

$$k_{\text{mix}}^{\text{R}} = 4 d_{p_{mix}}$$
$$\sigma T^3 \left\{ 0.5756 \epsilon_{\text{mix}} \tan^{-1} \left[1.5353 \left(\frac{k^{(\text{s})}}{4 d_{p_{mix}} \sigma T^3} \right)^{0.8011} \right] \right.$$
$$\left. + 0.1834 \right\} \quad , \tag{A19}$$

where

$$\epsilon_{\text{mix}} = \left[\sum_i \left(\frac{\epsilon_i^{(\text{s})} \phi_i^{(\text{s})}}{d_{p_i}} \right) \right] \Big/ \sum_i \left(\frac{\phi_i^{(\text{s})}}{d_{p_i}} \right)$$

$$i = \text{Ti, C, TiC, Diluent} \quad . \tag{A20}$$

It is worth noting that the hypotheses underlying the development of the Eqs. (A15) and (A19) fully agree with the assumptions introduced to develop the model discussed in the present work.

E. Volumetric fractions

In order to determine the volumetric fraction of the different phases and components involved in the system the following expressions have been used:

$$\left. \begin{aligned} \phi_i &= \phi_i^{(\text{s})} + \phi_i^{(\text{liq})} \\ \phi^{(\text{j})} &= \phi_A^{(\text{j})} + \phi_B^{(\text{j})} + \phi_C^{(\text{j})} + \phi_D^{(\text{j})} \\ \phi_i^{(\text{j})} &= \frac{m_i^{(\text{j})}}{\rho_i^{(\text{j})}} \end{aligned} \right\}$$
$$i = \text{Ti, C, TiC, Diluent}; \, j = \text{s, liq, gas} \quad . \tag{A21}$$